



The effect of wind environment on temperature and performance of an open-cathode proton exchange membrane fuel cell stack

Changjian Wang^{1,3} · Hongsheng Ma^{1,2} · Shuqi Duan^{1,2} · Weiping Zhao^{1,2}

Received: 12 November 2023 / Accepted: 8 July 2024 / Published online: 3 August 2024
© Akadémiai Kiadó, Budapest, Hungary 2024

Abstract

In practical applications, the proton exchange membrane (PEM) fuel cell stack is often exposed to wind environment, and the speed and direction of the ambient wind are random. The performance variation of an open-cathode PEM fuel cell under various ambient wind directions and speeds was studied. The results show that when the ambient wind direction is opposite to the cathode reactant or from the side of stack, the stack temperature increases and the stack power decreases finally. Moreover, with the increase in the wind speed, the running time of the stack is shortened significantly. For the ambient wind in the same direction as the cathode gas, the stack power increases at a high current and decreases at a low current. For the given speed and direction of ambient wind, the increased air flow rate of fan could alleviate the interference of ambient wind on the stack performance and temperature. However, while the stack temperature is more than the allowable maximum operating temperature, the stack power declines even though the air flow rate of fan increases.

Keywords Open-cathode PEM fuel cell · Temperature distribution · Output power · Ambient wind · Voltage uniform

Introduction

With the development and progress of science and technology, the demand for energy is growing. The development and application of renewable energy have also become a popular direction in various research fields. Nowadays, the proton exchange membrane (PEM) fuel cell stack is in the spotlight for cleanliness and high efficiency, and the products of PEM fuel cell on the market have become more mature and diverse [1–3]. The open-cathode PEM fuel cell system removes the need for a cooling water system, which greatly simplifies the system and reduces maintenance and fabrication costs [4]. The open-cathode PEM fuel cell has been widely used in emergency power sources, small electric

vehicles, unmanned aerial vehicles (UAV), and other fields as low-power source [5, 6].

For the PEM fuel cell, the effects of stack structures, air intake strategies, and the state parameters of the reaction gas on the stack performance and efficiency have been extensively studied. Some fuel cells adopt the dead-end anode gas control strategy, in which the anode exit is blocked so as to improve the hydrogen utilization rate. However, the insufficient fuel due to the blocked anode might cause the performance degradation and unstable cell voltage [7]. Han et al. [8] divided the anode cells of the battery pack into several blocks and operated it in the dead-end anode mode. It is found that the hydrogen utilization rate is greatly improved and the fluctuation of cell voltage becomes smaller. Hwang et al. [9] installed two valves in the hydrogen recirculation pipeline to make the anode gas run in different modes. It is found that the recirculation mode could effectively increase the cycle time. Yang et al. [10] fabricated an open-cathode stack with six single cells stacked in a stair configuration manner and concluded that this structure can provide more uniform and sufficient oxygen for the entire stack. Atkinson et al. [11] prepared a less porous gas diffusion media and applied it to the stack cathode, and found that the ohmic resistance of proton exchange membrane was greatly reduced. Kreesaeng et al. [12] established a mathematical

✉ Changjian Wang
chjwang@hfut.edu.cn

¹ College of Civil Engineering, Hefei University of Technology, Hefei 230009, Anhui, People's Republic of China

² Anhui International Joint Research Center on Hydrogen Safety, Hefei 230009, People's Republic of China

³ Engineering Research Center of Safety Critical Industrial Measurement and Control Technology, Ministry of Education, Hefei, People's Republic of China

model of PEM fuel cell to study the influences of cross-sectional area and aspect ratio of cathode flow channel on PEM fuel cell. It is found that the performance decreases with the increase in cross-sectional area, but improves with the increase in aspect ratio. Kiattamrong et al. [13] fabricated a PEM fuel cell of which the active area is 100 cm^2 , and explored the effect of six different geometries of air flow channels on the stack performance. The results show that the high aspect ratio flow channel had better performance, but the flow area had weak impact on stack. Zhao et al. [14] studied the impact of the cells number and bolt torque on the stack and found a range of the cells number within which the stack had the best performance and stability. Zhao et al. [15] made a 11-cell PEM fuel cell stack with a spoiler in the gas inlet system and reported that the spoiler can promote the stack performance. Moreover, the influence of position of the fan on stack performance was studied. It was found that the proper position of fan could promote the dissipation of heat. Strahl et al. [16] established a dynamic multiscale PEM fuel cell model and analyzed four different catalyst layer structures. It is found that only secondary pores model shows a better performance.

For open-cathode PEM fuel cell, it is also worth investigating the operating parameters of the stack. Zhao et al. [17] made a PEM fuel cell with 50 cm^2 active area, experimentally studied the optimum operating conditions of hydrogen pressure, temperature, humidity, and stoichiometric ratio for this stack. The results show that the suitable operating parameters could effectively improve the stack power. Xu et al. [18] investigated the effect of the reactant humidity on the PEM fuel cell for the case of the operating temperature 90°C . It is found that the stack performance with low humidity is better at the high current density. Meanwhile, compared with the anode gas, the effect of cathode reactant humidity on stack performance was more obvious. Combining the experimental and simulation results, Sachinet et al. [19] reported that the increased temperature and working pressure were beneficial to stack power, while the increase in stack operating temperature monotonously led to dehydration of the membrane. Yang et al. [20] built a comprehensive transient multi-dimensional model of PEM fuel cell system and found that the water production of the stack increased with the stack current, while the increased stoichiometric ratio of air made the generated water be removed so quick that membrane dehydration was accelerated. Lu et al. [21] explored the influence of back pressure on stack performance. It turned out that high back pressure would increase the water content of PEM, so the stack voltage was improved. Each current density had a corresponding optimal back pressure. When the back pressure reached the optimum value, the promoting impact of back pressure on the stack voltage gradually disappeared. Zhang et al. [22] reported that although the high back pressure improved the stack

performance, the stability of the current distribution was worse. The poor performance always occurs at the outlet, where it is prone to water accumulation and air consumption. It can be found that the operating parameters resulted in the changes of heat and water caused by the fuel cell; thus, the stack power was affected. Therefore, the water and thermal management were very important to the stack performance.

In practical applications, PEMFC is often exposed to the natural environment, so it inevitably needs to be operated under some extreme conditions. As a matter of fact, many researches focus on the effect of the environmental temperature on the performance of fuel cells. Williamson et al. [23] investigated the effect of ambient temperature on air-cooled PEMFC using the polarization scanning. They found that the performance of cathode-open PEMFC stacks depends on the stack temperature, while the temperature distribution of closed structure cells is more balanced. Pahon et al. [24] investigated the performance differences of open-cathode PEMFC stacks at different ambient temperatures. Two environmental temperatures are considered, namely a constant room temperature of 20°C and a temperature range of -30 to -2°C . The results indicate that due to inevitable water freezing inside the fuel cell, the performance of fuel cells stored for a long time at low temperatures deteriorates more compared to those stored at a constant room temperature. Hottinen et al. [25] investigated the cold-start behavior of PEMFC stacks under sub-zero temperature conditions and observed the phenomenon of external icing on the cathode side and irreversible loss of stack performance. Zeyoudi et al. [26] evaluated the performance of cathode-open PEMFC stacks under environmental temperatures in the Abu Dhabi region. The experimental results show that the output power of the fuel cell stack is about 40% lower in summer than that in winter. This is because the high temperature environment in summer can cause membrane dehydration and reduce its ion conductivity, thereby weakening the performance of the stack. Wilson et al. [27] thawed the PEM fuel cell after freezing it three times and found that the stack performance was not significantly deteriorated. Cho [28] also conducted a freeze–thaw experiment of PEM fuel cell and found the distribution of ice could affect the stack current. It was believed that the ice first appeared in the cathode catalyst layer. When the temperature inside the stack can melt the ice layer, the stack successfully starts. Oszcipok et al. [29] conducted cold-start experiments of PEMFC at ambient temperatures of -10 and -20°C . The results show that above -10°C the stack was able to be started, and the resistance of membrane had an obvious effect on the starting behavior. Zhang et al. [30] tested the stack under three different radiation intensities and found that the stack power decreased rapidly with the intensification of the radiation intensity, and then, the operation stopped automatically. Atkinson et al. [31] put the open-cathode PEM fuel cell in

an indoor wind tunnel to simulate actual atmospheric flight conditions. It also studied the performance of the stack under wind speed and altitude. It was found that the stack power was lost 38% when the wind speed decreased from 15.4 to 0 ms^{-1} , and the stack voltage and power were lost at high altitude. It might be related to the oxygen partial pressure and temperature at a high altitude.

The previous studies on the effect of the environmental temperature on the PEMFC stacks were relatively comprehensive. However, the environmental factors include not only temperature, but also factors such as radiation, electromagnetism, and wind. At present, the focus on the effect of wind speed and direction on PEMFC performance is rarely little. As a matter of fact, the interference of ambient wind is inevitable for the working environment of open-cathode PEMFC stacks. Although Atkinson et al. [31] reported the effect of wind speed on stack, the experimental conditions were simple. When the open-cathode PEM fuel cell is used in UAVs as a power source under the ambient wind, the

intensity and direction of the ambient wind are random. The direction and speed of environmental wind may affect the air intake parameters and heat dissipation of cathode-open fuel cell stacks, thereby affecting the performance of fuel cells. Therefore, the purpose of this article is to investigate the effects of the ambient wind with different intensities and directions on the output power, operating temperature, and voltage of fuel cells.

Experimental

Experimental platform

In experiment, a 20-piece open-cathode PEM fuel cell stack is selected, and the parameters of experimental stack are shown in Table 1. It is worth noting that the small unmanned aerial vehicles typically carry fuel cell stacks of several hundred watts [32–36]. Therefore, a low-power stack is used to investigate the effect of environmental wind on the performance of the stack in this study. The specific experimental platform is presented in Fig. 1. After the solenoid valve of the hydrogen circuit is opened, the hydrogen pressure and volume are regulated by the valve and the hydrogen flow rate controller. Then, the hydrogen is sent to the stack to react with the air, followed by the discharge of the exhaust gas. In experiment, the dead-end anode mode is set by a solenoid valve installed at the exhaust port to control the on/off, and the time relay of 20 s is used to open the solenoid valve to discharge exhaust gas in a time of 0.2 s. The solenoid valve, hydrogen flow rate controller, temperature, and humidity

Table 1 Parameters of the experimental stack

Parameters	Value
Dimension /mm	200×60×120
Mass /g	1948
Cells number /-	20
Active area / cm^2	130
H_2 inlet pressure /MPa	0.08
Rated power /W	360
Normal operating temperature / $^{\circ}\text{C}$	50

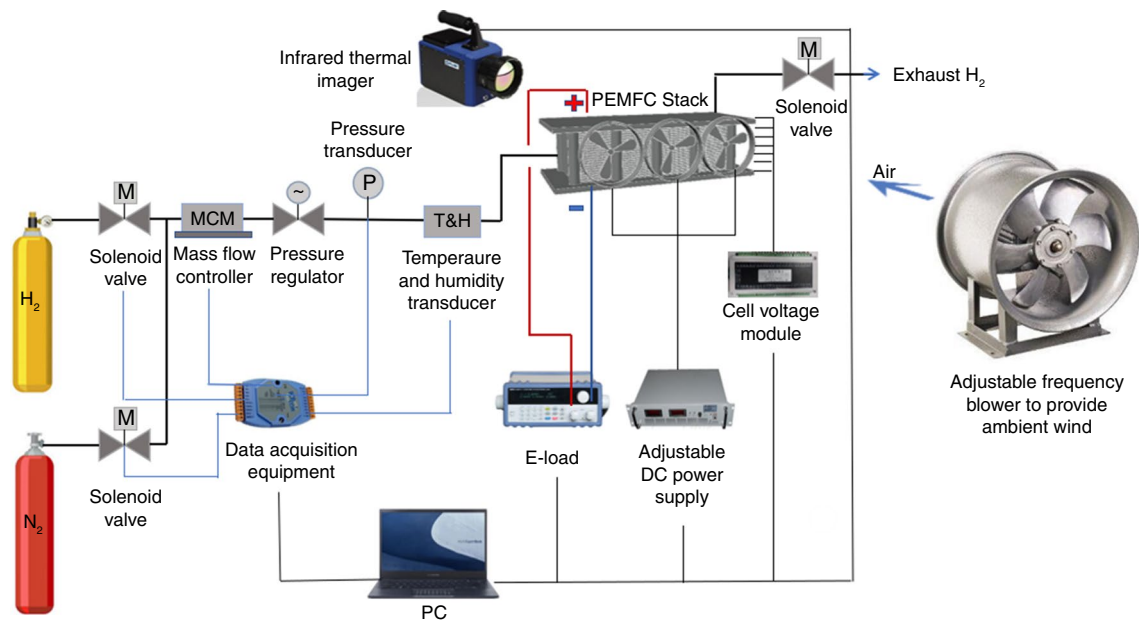


Fig. 1 Diagram of experimental platform

sensors transmit the collected data to the computer through the information acquisition module for synchronous control and data monitoring.

Measurement system

The cathode gas is supplied by two axial flow fans with dimensions of $90 \times 90 \times 35$ mm and voltage range of 7–14 V, as well as the stack cooling. The voltage of the axial flow fan is controlled by an adjustable DC stabilized power supply. In order to accurately measure the wind speed, five fixed monitoring points are set in the wind field. The wind speed at each monitoring point for different fan frequencies is sequentially measured using an anemometer. The average value is taken as the wind speed under each experimental condition. In Table 2, the corresponding air flow rate and the air speed of fan are presented.

The positive and negative electrodes of the stack are connected to an adjustable DC electronic load. Different load currents can be set in constant current mode on the computer. Meanwhile, the stack voltage and power are measured. A single voltage acquisition module is inserted between each single cell to record its voltage evolution.

In previous studies, the thermocouples [30, 31, 37–43] and infrared thermal imager [14–17] were used to obtain the stack temperature profiles. Because the inserted thermocouples may block the cathode channel and affect the uniformity of the ambient wind, an infrared camera is installed at the entrance of the stack to measure the temperature.

Table 2 Voltage, air flow rate, and air speed of the fan

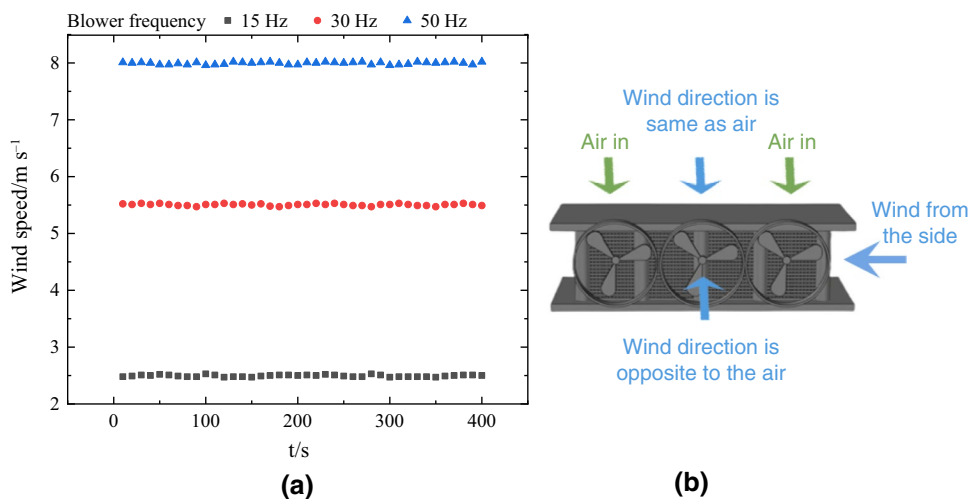
Voltage/V	8	10	12	14
Air speed/ ms^{-1}	1.12	1.28	1.46	1.65
Air flow rate/CFM	106.50	133.87	160.22	187.13

In order to achieve a uniform environmental wind field, a rectifier device is installed at the outlet end of the blower frame. The device is composed of orderly stacked polyethylene plastic hollow circular pipes with a radius of 5 mm. After rectifying the turbulent airflow from the blower, a laminar airflow suitable for quantitative analysis is output. The uniformity of the wind field can be proved by the wind speed data in Fig. 2a. For a given blower frequency, the wind speed stabilizes at a constant value over time. Moreover, the stack is set at a horizontal distance of 60 cm from the air outlet of the blower, and the stack is kept at the same height as the wind to ensure that the whole stack is in the wind field in experiment. The wind speeds of 2.5, 5.5, and 8 ms^{-1} are selected according to the distribution of wind resources and the Beaufort wind scale [39–41]. The ambient wind speed is shifted by the frequency regulator of the blower. Figure 2a shows the wind speed evolution at the measuring point within 400 s under three different blower frequency. Although the real wind pattern is random, three representative wind directions are considered in experiment, namely the same as the cathode intake direction, opposite to the cathode intake direction and from the side of the stack, as shown in Fig. 2b. The selection of these three typical directions is meaningful, as the cathode gas parameters and stack heat dissipation are significantly affected.

Experimental procedure

Before each experiment, the environmental temperature and humidity are both recorded to ensure that the temperature of each experiment is basically $24 \text{ }^\circ\text{C}$ ($\pm 2 \text{ }^\circ$) and the humidity is 40% ($\pm 3\%$). Firstly, the solenoid valve of nitrogen circuit is opened to purge the stack for three minutes, and then, the speed of the blower is adjusted by the frequency regulator. After the blower runs for one minute, the voltage of the cooling fan is set. The solenoid

Fig. 2 Wind parameters: **a** profiles of the wind speed at the horizontal center of the stack under three different blower frequency; **b** three selected ambient wind directions



valve of the hydrogen circuit is shifted to keep the pressure of the hydrogen 0.08 MPa. The stack runs for 6 min with the current of 5 A after the stack open-circuit voltage is stabilized. Then, the current is increased by 5 A to run for another 6 min until the stack cannot run stably, and the electronic load and the stack could be stopped running. After the stack temperature returns to normal values, the frequency and voltage of the fan are changed to carry out the next experiment.

Experimental results and discussions

Effect of ambient wind direction

In Fig. 3, the variations in the stack power and maximum temperature are revealed. When it was exposed to the ambient wind in different direction, the stack power and temperature changed significantly.

As shown in Fig. 3a, when the stack was exposed to the ambient wind which is in the same direction as the stack cathode gas, the stack power shows a more obvious down-trend compared with that without ambient wind, which is

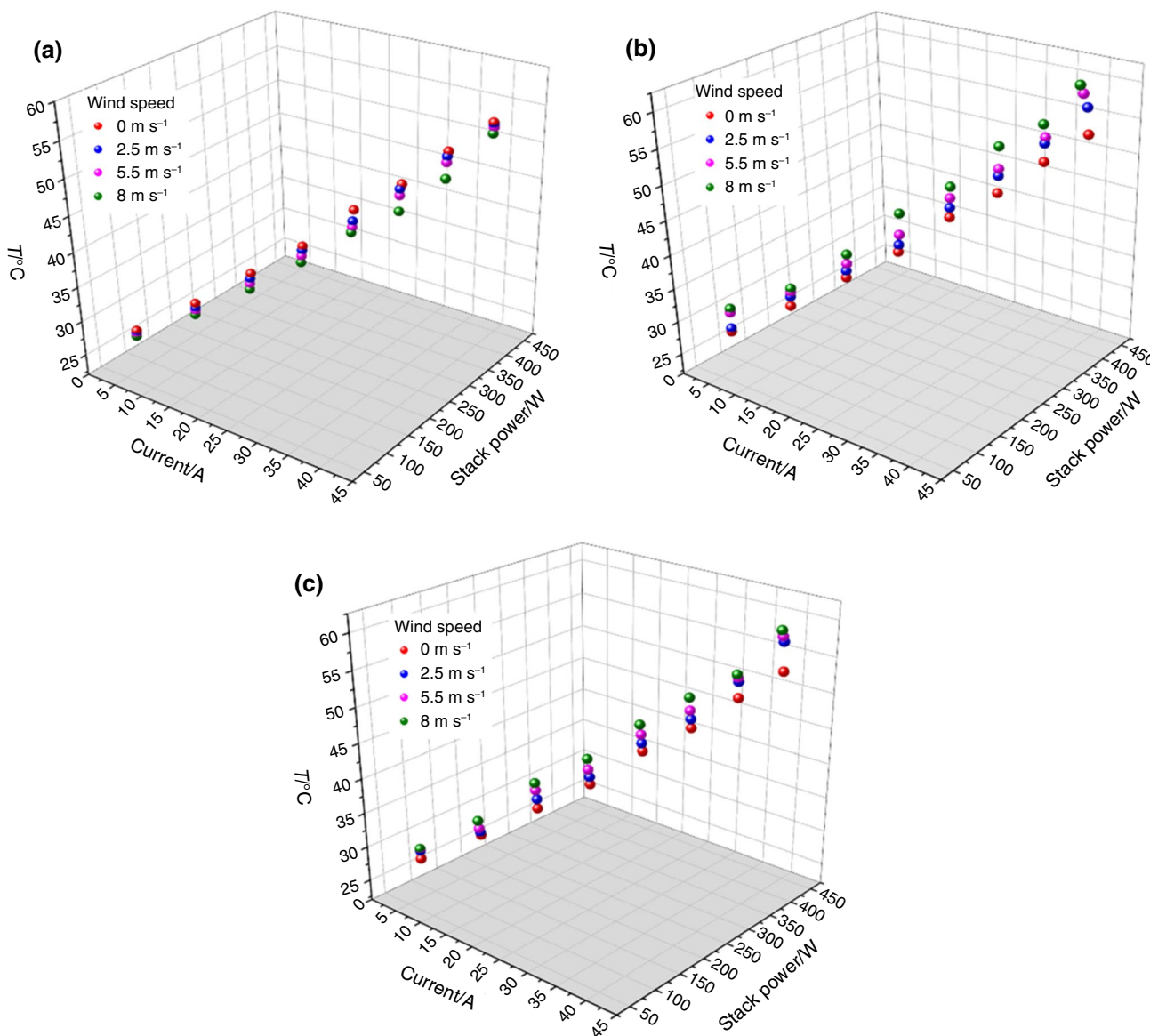


Fig. 3 Variations in stack power and maximum temperature under ambient wind from different directions (air flow rate of fan: 187.13 CFM), **a** the direction of the ambient wind is same as the

cathode gas; **b** the direction of the ambient wind is opposite to the cathode gas; **c** the direction of the ambient wind is from the side of the stack

related to the difference of stack temperature. It could be observed that the maximum stack temperature with ambient wind is significantly lower than that without ambient wind. Since the ambient wind is in the same direction as the stack cathode gas, the heat dissipation and the flow rate of the cathode gas are accelerated. Therefore, the temperature rise rate decreases, and the stack operating temperature becomes lower. The stack power decreases as the temperature decreases, which is associated with the stack water and thermal management. The temperature and water content of the PEM are the main factors that influence the PEM fuel cell stack, and each stack has its optimum operating temperature [17]. When the stack temperature is below the optimum operating value, the voltage increases with the temperature of the stack. Correspondingly, the voltage gets lower when the stack temperature decreases [19]. It could be interpreted as a decrease in the activity of the catalytic layer at low temperatures, as well as a decrease in the hydration level and conductivity of PEM [20]. The PEM ohmic resistance increases accordingly when the stack temperature decreases [44], and the degraded power of stack is induced. When the current of the cell stack is loaded from 5 to 35 A, the effect of environmental wind on the power of the stack becomes more significant as the current increases. This can be explained by the fact that the less water and heat are produced in the stack regardless of the ambient wind interference exists or not for the case of low current density. Therefore, the proton exchange membrane is not hydrated evenly. Moreover, the gas diffusion layer may be blocked by the water as it is difficult to be evaporated at a low temperature. Consequently, it leads to difficulties in mass transfer [45]. However, the water in cathode channel could be properly taken away by the ambient wind, so the power difference of the stack is small at low current. When the load current increases, the temperature and water produced by stack increase as well, which causes the hydration of the PEM become better [46]. But the excessive heat dissipation is caused by the ambient wind, and the high air velocity takes away the water produced by the stack. As a result, the water inside the PEM is lost, and the difference of stack power increases. When the current rises to 40 A, the power of the stack under ambient wind is basically the same as that without ambient wind. The reason is that the stack produces much more heat under high current, and the stack temperature could exceed the optimal operating temperature (50 °C). Without the ambient wind, the cooling capacity of the fan is not enough so that the heat accumulation is induced. Therefore, the local overheating of the stack occurs so that the stack power decreases. However, the ambient wind in the same direction as the cathode gas can take away the heat produced by the stack. As the wind speed increases, the stack temperature can be reduced to a normal range, and the evaporation rate of water in the membrane at high temperature is reduced, and also the operating

time of the stack is effectively promoted. Moreover, the rate of water production is lower than the evaporation rate of the stack at high temperature. The water loss of the membrane leads to the decrease in stack performance. Therefore, it can be concluded that generally, environmental winds in the same direction as the cathode gas result in a negative impact on the stack. However, for the case of the high current, the water and thermal management is improved effectively, and the maximum power and operating time of the stack increase.

As presented in Fig. 3b, when the direction of the ambient wind is opposite to the cathode gas, compared to no ambient wind, the output power of stack firstly improved and then degraded. According to the maximum stack temperature, it can be found that ambient wind in the opposite direction to the cathode gas has a remarkable heating effect on the stack. For the air-cooled fuel cell, the cathode gas is involved in the reaction, and the temperature decay of the fuel cell stack is due to the forced convection of heat generated during the operation of the stack. The exhaust side of the stack is blocked by environmental winds that are opposite to the cathode reactants. The heat cannot be dissipated because the gas with heat encounters the airflow in the opposite direction at the air outlet, so the stack temperature rises. When the stack temperature rises, the mass transfer capacity of PEM and the thermal motion of reactant are accelerated. Simultaneously, the rise of stack saturated vapor pressure occurs, and the hydration of the PEM is enhanced [46, 47]. Moreover, the ohmic resistance of PEM also decreases [44] with the rise of stack temperature, and therefore, the stack performance is enhanced. When the load current rises to 35 A, the power differences of the stack with and without ambient wind are smaller, even the maximum stack temperature is much higher compared with that without ambient wind. When the current is 40 A, the stack power is even lower than that without the ambient wind. Since the heat dissipation is hindered under the interference of ambient wind, the stack temperature increases caused by the heat accumulation. Eventually, the dehydration of the membrane results that the stack performance is degraded [43]. The heat produced by the stack under the high current can be discharged through the forced convection of the fan, so that the maximum stack temperature is basically maintained at the optimal range of stack temperature.

As shown in Fig. 3c, the stack power in the scenario with lateral environmental winds is significantly lower than that in the scenario without environmental winds. Moreover, the degradation amplitude gradually increases with the current. The degradation of the power is often associated with the water and thermal management. Moreover, the degradation is accompanied by the abnormal rises of stack temperature or uneven heat distribution [43]. According to the maximum temperature of the stack, it can be found that when the

ambient wind is from the side, the maximum stack temperature increases than that without the ambient wind. With the current ranging from 5 to 30 A, the maximum stack temperature is below the optimal stack temperature. As mentioned above, the stack temperature is positively correlated with the stack performance. The degradation of power seems to contradict the theory. When the ambient wind is from the side, the supply of the cathode gas is insufficient because the inlet and outlet of stack are hindered. Consequently, the uniformity of the gas distribution is also deteriorated. It means that the heat produced by the stack cannot be dissipated evenly. Therefore, the local overheating occurs and the heat management is worsened. In addition, the amount of reaction air in some areas of the stack is insufficient because the reactant cannot distribute uniformly in flow channel. Hence, a large difference of current density in different parts is caused by the local oxygen starvation. Moreover, the negative and positive electrodes are reversed, and the high temperature of the stack may happen, which leads to the local degradation of membrane electrode assembly [48]. It is the reason that the stack power decreases with the increase in stack temperature.

Effect of ambient wind speed

The ambient wind speed is also considered to further discuss the influence of ambient wind on the stack. Figure 4 presents the variation in the operating time of the stack with the wind speed under different direction of ambient wind. Figure 4 shows when the stack is exposed to the ambient wind in the same direction as the cathode gas, the operating time of the stack increases gradually with the

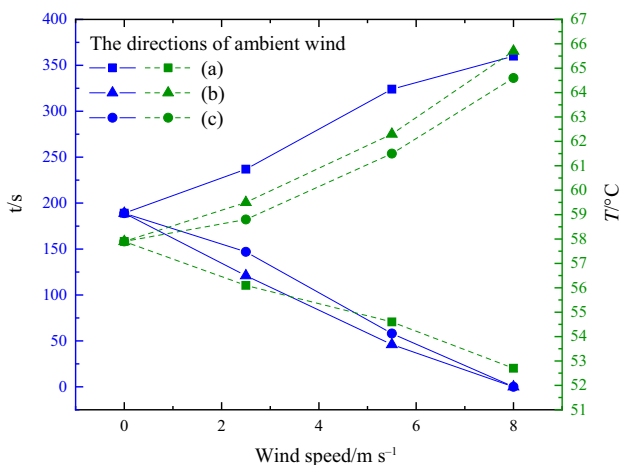


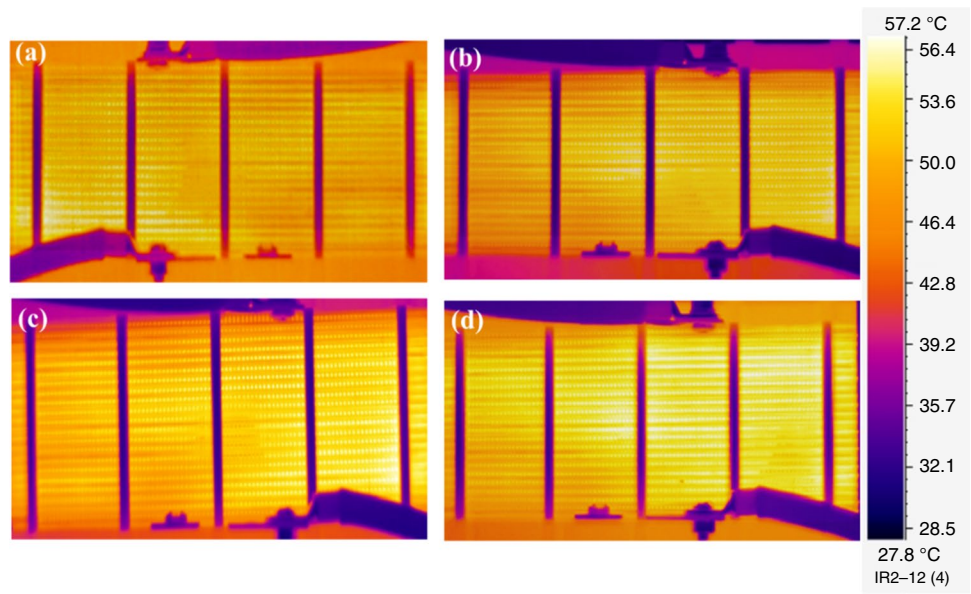
Fig. 4 Variation in the operating time of the stack with the wind speed under different ambient wind directions (air flow rate of fan: 160.22 CFM, load current: 40 A), **a** the direction of the ambient wind is same as the cathode gas; **b** the direction of the ambient wind is opposites to the cathode gas; **c** the direction of the ambient wind is from the side of the stack

ambient wind speed. Furthermore, the forced convection of the ambient wind on the outside of the stack is strengthened, so the air volume in channel and the heat dissipation increase. Therefore, the stack temperature gradually drops to a normal value, and the operating time of the stack increases accordingly.

As shown in Fig. 4, when the direction of the environmental wind is opposite to the cathode gas or when the environmental wind comes from the side, the operating time of the stack is gradually shortened with the increase in the ambient wind speed. However, the reasons for the decay of the operating time of the stack in these two cases are different. When the direction of the ambient wind is opposite to the direction of the cathode gas, due to the heat dissipation being blocked, the effect of the ambient wind on the outlet of cathode gas increases with the wind speed. Consequently, the heat is more likely to be accumulated in the stack, and the increase in temperature has a certain promotion impact on the stack even at a low current. Moreover, the more heat of stack can be produced at a high current. When the stack temperature is enough high to damage the PEM, the stack stops running. The magnitude of the degradation decreases gradually as the wind speed increases. The reason is that without the ambient wind, the optimal stack temperature has been exceeded. However, as the speed of ambient wind that opposite to the cathode gas increases, the stack temperature still rises due to the heat accumulation. When the maximum stack temperature is over 65 °C, the stack cannot continue running. When the wind speed reaches the maximum value of 8 m s⁻¹, the stack stops running directly at 40 A. As a consequence, the operating time of the stack is 0 s, which results in a decreasing trend in the attenuation amplitude of the stack.

In Fig. 4, when the ambient wind blows the stack from the side, the interference of ambient wind on the stack increases with the wind speed. Moreover, the heat dissipation of stack becomes more difficult, and the cathode reactant is reduced so that it cannot be distributed in the flow channel evenly. The differences of heat generation and current density in various parts of the stack increase gradually. Figure 5 presents the variation in temperature distribution with wind speed for the case of the ambient wind from the side. Apparently, the phenomena of local oxygen starvation and uneven heat dissipation in the stack become more obvious with the increase in wind speed. Therefore, the duration of high temperature degradation of the membrane electrode may be shortened, and the heat is easier to be accumulated inside the stack. Similarly, when the load current of the stack is loaded at 40 A, the operating time of the stack decays greatly and drops to 0 s directly.

Fig. 5 Variation in temperature distribution with wind speed for ambient wind from the stack side (air flow rate of fan: 160.22 CFM, load current: 35 A), **a** 0 ms⁻¹; **b** 2.5 ms⁻¹; **c** 5.5 ms⁻¹; **d** 8 ms⁻¹



Effect of air flow rate of the fan

As mentioned above, the influence of ambient wind on the stack cannot be ignored. In order to alleviate the interference of ambient wind in practical applications, the air flow rate of the fan is changed to explore the influence on the stack under the ambient wind.

Figure 6a shows that when the ambient wind is in the same direction as the cathode gas, the degraded power of the stack increases with the current, then drops sharply after reaching the peak value, and finally shows a negative value, which means the increase in stack power. As the air flow rate of fan rises, the degraded power of stack increases. After the

maximum value is reached, the rise of air flow rate of fan also slows the downtrend. In Fig. 6b, the degraded power is caused by the decrease in temperature, and the heat dissipation is accelerated with the increase in the air flow rate of fan. Thus, the degraded power of the stack also increases. In the absence of ambient wind, the power of the stack begins to decrease as it reaches its maximum temperature. Under the interference of the ambient wind, the temperature of stack is near the optimum value at same working conditions. As a result, the degraded power of the stack begins to decline, and a peak can be found, followed by a negative value. When the air flow rate of fan increases, regardless of the presence of ambient wind, the temperature of the stack

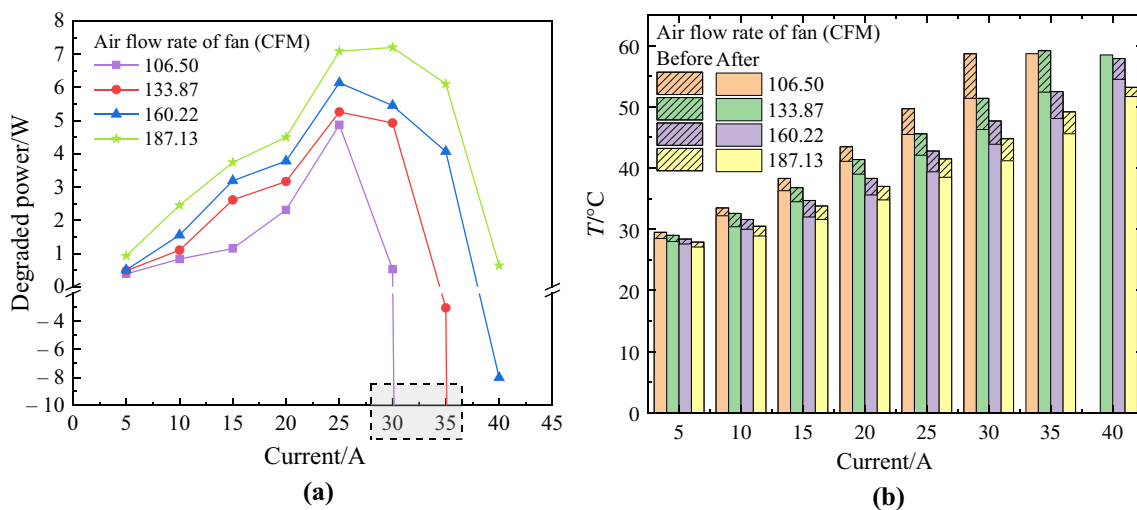


Fig. 6 For the ambient wind in the same direction as the cathode gas, the influence of current on (wind speed: 8 ms⁻¹), **a** the degraded power; **b** the stack temperature, ?before? means that without ambient wind; ?after? means that with ambient wind

decreases. The duration of the stack temperature to achieve the maximum operating temperature or the optimal operating temperature also is prolonged, and the decreasing trend of the degraded power of the stack is slowed down. It should be pointed that, in the gray area in Fig. 6a, the air flow rate of fan is 106.50 and 133.87 CFM; the degraded power of the stack directly reaches a minimum value when load current increases. The value is not expressed because it is too small, but marked with a gray area specially for explanation. Combined with Fig. 6b, without the interference of ambient wind, the temperature is about 60 °C while the air flow rate at 106.50 CFM and the current at 30 A. So as to the air flow rate of fan at 133.87 CFM and the current at 35 A. Because the temperature is over the optimal value, the fuel cell is unable to run stably. However, with the ambient wind, the maximum temperature can be reduced to about 50 °C. Thus, for the cases of the air flow rate of fan at 106.50 and 133.87 CFM, the maximum load current required for the operation of the stack increases to 30 and 40 A, respectively. The operating time and output power of the stack increase significantly, which means that the maximum power of the stack can reach 386.706 and 412.232 W, respectively. Due to the large difference with other data, it is marked and explained separately.

Similarly, in Fig. 7a, when the stack is interfered with the wind in opposite direction to the cathode reactant, the variation in the increased power with the current is focused with different air flow rate of fan. It should be noted that since the ambient wind affects the stack power positively, the increased power of the stack (stack power with ambient wind interference?stack power without interference) is selected as the Y-axis parameter. The overall curve is basically the same as that in Fig. 6a, which means that the increased power first increases to the peak value

and then drops sharply. With the rise of air flow rate of fan, the increased power of stack decreases, and the peak value of the curve is shifted back gradually. Figure 7b presents that the temperature increases with ambient wind. While the current increases, the temperature difference between with and without ambient wind increases, so the increased power of the stack shows an upward trend. With ambient wind, the maximum stack temperature can be achieved, and the power of stack begins to be attenuated. While without ambient wind, the stack temperature approaches the optimal operating temperature gradually, the stack power reaches the maximum value. Therefore, the increased power of the stack appears to be a maximum value. As the current continues to increase, the increased power of the stack drops to a negative value, which means that the stack power with ambient wind is lower. When the air flow rate of fan increases, the difference of temperature with and without the ambient wind gradually decreases. Because the air flow rate can alleviate the hindering effect of the ambient wind on the heat dissipation, the speed of temperature rise for the stack slows down with the ambient wind. Therefore, the increased power of the stack decreases with the difference of the temperature, and the deceleration of the temperature rise rate also effectively prolongs the duration for the stack to reach the maximum operating temperature. The gray area in Fig. 7a represents that while the current increases, the increased power still decreases. Without the ambient wind, the stack power can be operated under the same working conditions, but with the ambient wind, the stack power decreases to 0 W due to the high temperature. As a result, the increased power has a significant negative value. Thus, it is not directly represented in Fig. 7a, but marked with a gray area specially for explanation.

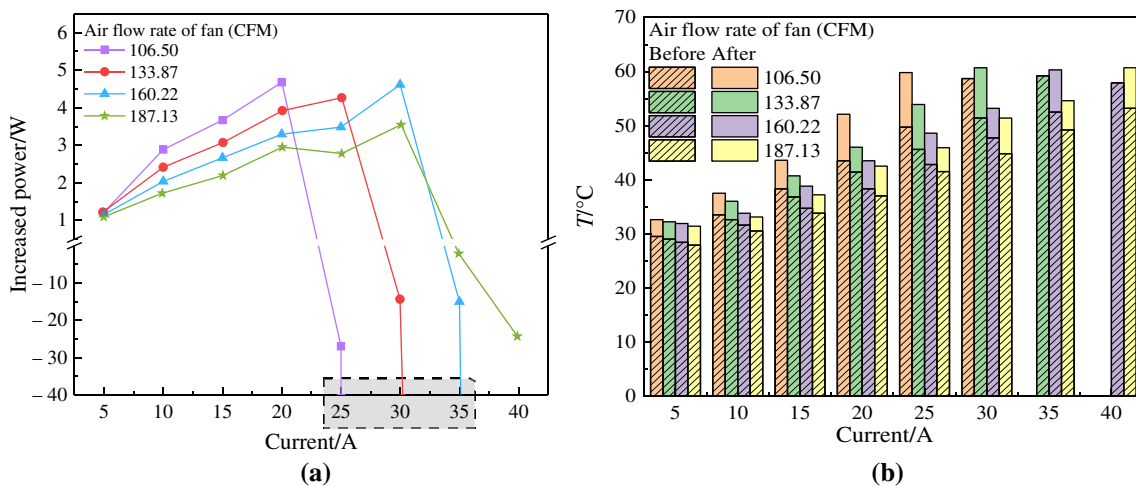


Fig. 7 For the ambient wind in the opposite direction to the cathode gas, the influence of current on (wind speed: 8 ms⁻¹), a the increased power; b the stack temperature, before means that without ambient wind; after means that with ambient wind

Figure 8 presents the effect of current on the degraded power and stack temperature for the ambient wind from the side. As shown in Fig. 8a, the degraded power varies with the current for the different air flow rate of fan. The degraded power presents a rising trend, and the rise of air flow rate causes the degraded power of the stack to decrease gradually. As seen in Fig. 8b, the stack temperature increases with the interference of ambient wind. However, according to the previous analysis, although the temperature of the stack increases, the internal current distribution of the stack is uneven. Thus, the power of the stack decreases.

From the above analysis, it can be concluded that the increase in air flow rate of fan effectively alleviates the degraded power of the stack. In order to characterize the voltage decay of the single cell, an important parameter C_v is used to evaluate the voltage distribution uniformity of the stack. The calculation formula for C_v is as follows [30, 32]:

$$C_v = \sqrt{\frac{\sum_{i=1}^n \left(\frac{U_i - \bar{U}}{\bar{U}}\right)^2}{n}} \times 100\% \quad (1)$$

where n is the cells number; U_i is the voltage of the i -th single cell; and \bar{U} is the average voltage of all single cells. A larger C_v means a more uneven voltage distribution of the single cells. In other words, an increase in C_v indicates an increase in voltage instability of the cell stack. Generally, a sudden increase in C_v also indicates the sudden attenuation of the voltage of one or more single cells. The lower C_v means the uniformity of the stack is better. Figure 9 presents the changes of C_v with time for the ambient wind from the side. The load current increases every 360 s, and the C_v is also terminated when the stack stops. A jump can be found on the C_v curve as the load current increases. As mentioned

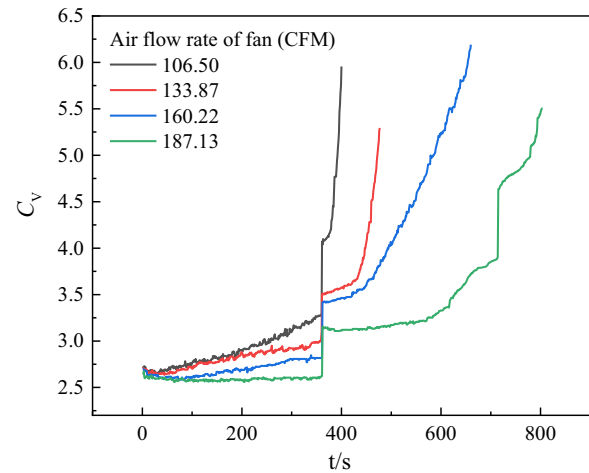


Fig. 9 Changes of C_v with time at different air flow rate of fan under the ambient wind from the side (wind speed: 8 ms^{-1})

before, the heat and water production inside the stack are promoted with the increase in current. The distribution uniformity of the inlet gas and outlet is affected by the ambient wind. It further leads to a decrease in the local temperature and water content for the proton exchange membrane. Therefore, the stack ultimately stops running. Moreover, with the increase in air flow rate, C_v decreases while the operation time of stack is extended.

Figure 10 presents the effect of air flow rate of fan on single-cell voltage and C_v under the ambient wind from the side. As shown in Fig. 10a, it can be concluded that the cell voltage fluctuates significantly, especially the rapid decrease in cell voltage of No.12, which leads to an increase in C_v . When the heat is dissipated by fan, the No.12 cell is at the position of blades and the channels are blocked. The ambient

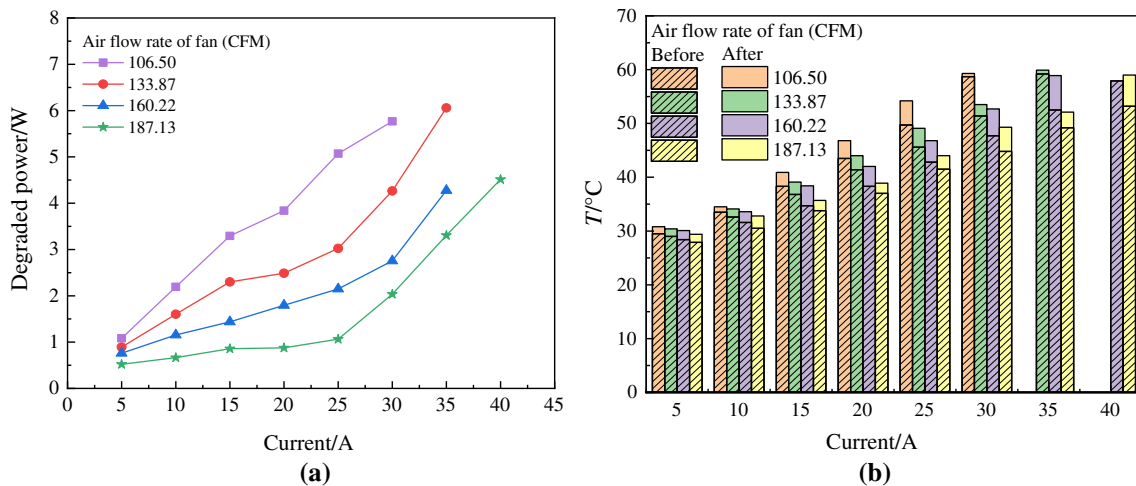


Fig. 8 For the ambient wind from the side, the influence of current on (wind speed: 8 ms^{-1}), **a** the degraded power; **b** the stack temperature, before means that without ambient wind; after means that with ambient wind

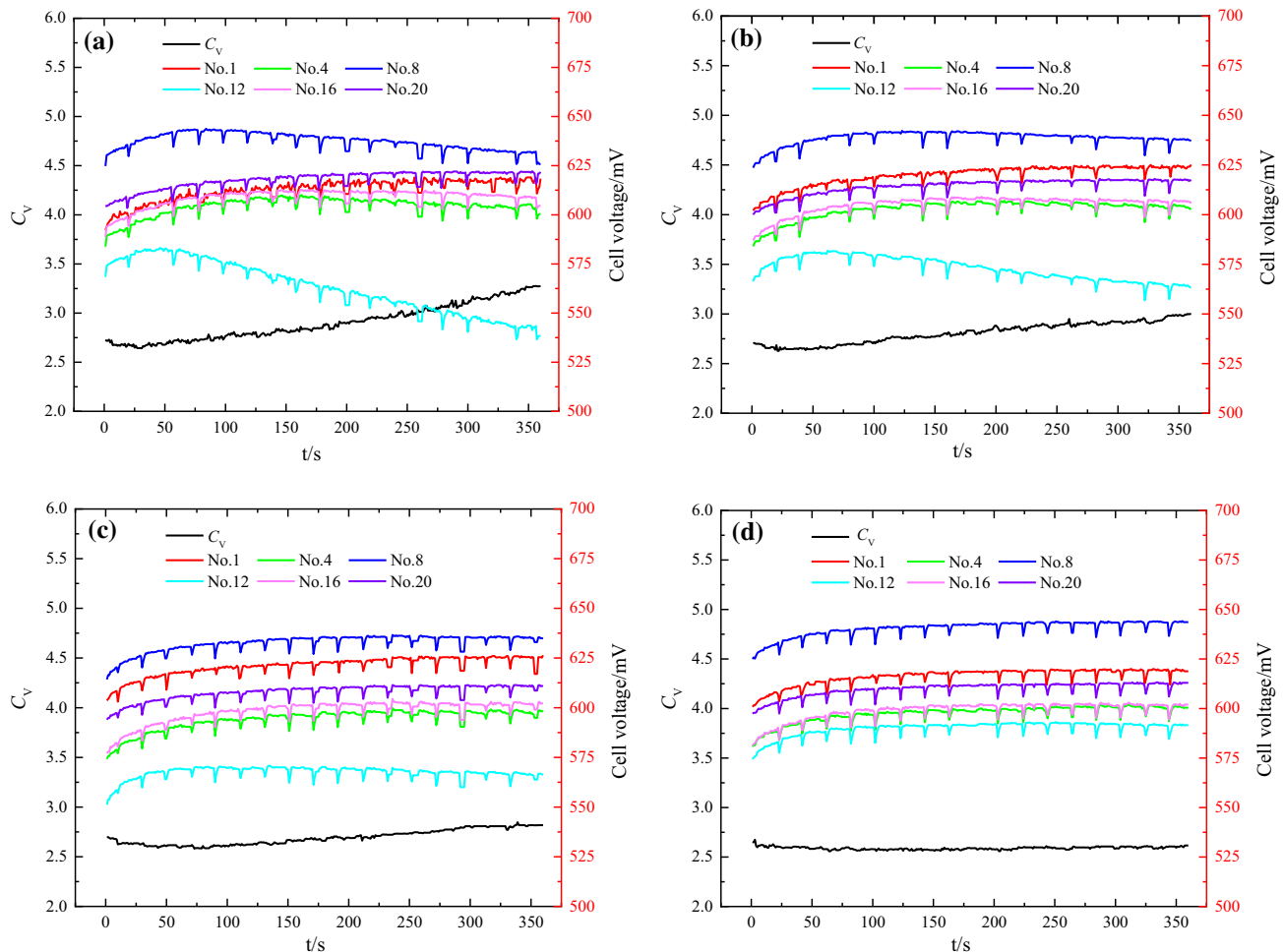


Fig. 10 Effect of air flow rate of fan on single-cell voltage and C_v under the ambient wind from the side (wind speed: 8 ms^{-1} , load current: 30 A), the air flow rate of fan: **a** 106.50 CFM; **b** 133.87 CFM; **c** 160.22 CFM; **d** 187.13 CFM

wind strengthens the uneven heat dissipation. Therefore, the more heat is concentrated in the cell No.12, which results in a decrease in cell voltage. Consequently, the stack cannot run sequentially. To compare with Fig. 10b, c and d, when the air volume increases, C_v and cell voltage become stable gradually. The interference of the ambient wind on No.12 is alleviated as the air flow rate in channel is accelerated. Thus, the distribution of cathode reactant is uneven and local high temperature of stack is weakened. With the stability of No.12 cell voltage, the voltage uniformity is enhanced. Therefore, the increase in air flow rate could mitigate the effect of ambient wind on the stack performance.

Conclusions

The effect of ambient wind on the open-cathode stack is studied. The stack performance at different ambient wind directions and wind speeds is tested. Moreover, the output

power, operating temperature, and voltage of stack are mainly discussed. The conclusions are summarized below.

- (1) For the ambient wind in the same direction as the cathode gas, the stack temperature is lower than that without ambient wind, and the stack power also shows a downward trend. When the current is increased, the stack can reach the higher power, and the operating time of the stack increases. When the ambient wind speed increases, the degraded power of the stack is more obvious at a low current, and the stack temperature is lower, but the operating time of the stack increases.
- (2) For the ambient wind direction opposite to the cathode reactant, the stack temperature increases. The stack power increases first and decreases finally compared with that without the ambient wind. When the ambient wind speed increases, the effect on the stack is more obvious. The maximum current that the stack can reach

is reduced, and the operating time of the stack is also significantly shortened.

- (3) For the ambient wind from the side, the inlet and outlet of stack are hindered, which results in the insufficient supply of the cathode gas. Consequently, the heat produced by the stack cannot be dissipated evenly due to the non-uniformity of gas distribution; meanwhile, the current density of each part significantly varies. Therefore, the voltage uniformity of the single cell is worsened affected by the local overheating, which further leads to a decrease in the stack power. As the wind speed and current increase, the degraded power of stack increases, and the running time of the stack is also shortened.
- (4) The increase in the air flow rate of fan can effectively alleviate the interference of ambient wind on the output performance and stack temperature. Especially the high current can benefit to improve the water and thermal management. Moreover, the duration for the stack to achieve the maximum operating temperature can be prolonged. However, when the stack temperature is too high to run stably, the stack power continuously decreases until the stack stops running even though the air flow rate is risen.
- (5) For a given load current and an air flow rate of the fan, when the environmental wind direction is the same as the cathode airflow direction, an increase in the wind speed can improve the operation performance of the fuel cell stack. For the scenarios where the environmental wind direction is opposite to the cathode airflow direction or comes from the side of the fuel cell stack, the fuel cell stack cannot run normally. As the wind speed increases, the operating time of the fuel cell stack decreases and the temperature of the fuel cell stack increases. When the wind speed reaches 8 ms^{-1} , the fuel cell stack cannot run.

Acknowledgements This study is supported by the National Natural Science Foundation of China (Grant No. 52171348) and the Fundamental Research Funds for the Central Universities of China (No. PA2023GDSK0046 and PA2023GDGP0044).

Author contributions CW involved in methodology, investigation, writing, validation, visualization; HM took part in investigation, experimentation, writing, validation; SD involved in resources, experimentation, writing review and editing; WZ participated in investigation, experimentation.

Declarations

Conflict of interest The authors declare that they have no known competing financial interests or personal relationships that could have appeared to influence the work reported in this paper.

Consent to participate and publish Informed consent was obtained from all individual participants included in the study. The participant has consented to the submission of the research content to the journal.

References

1. Niakolas DK, Daletou M, Neophytides SG, Vayenas G. Fuel cells are a commercially viable alternative for the production of clean energy. *Ambio*. 2016;45:327. <https://doi.org/10.1007/s13280-015-0731-z>.
2. Mehta V, Cooper JS. Review and analysis of PEM fuel cell design and manufacturing. *J Power Sources*. 2003;14:3253. [https://doi.org/10.1016/S0378-7753\(02\)00542-6](https://doi.org/10.1016/S0378-7753(02)00542-6).
3. Wang Y, Chen KS, Mishler J, Cho SC, Adroher XC. A review of polymer electrolyte membrane fuel cells: technology, applications, and needs on fundamental re-search. *Appl Energy*. 2011;88:981–1007. <https://doi.org/10.1016/J.APENERGY.2010.09.030>.
4. Kim K, Kim T, Lee K, Kwon S. Fuel cell system with sodium borohydride as hydrogen source for unmanned aerial vehicles. *J Power Sources*. 2011;196:906–975. <https://doi.org/10.1016/j.jpowsour.2011.01.038>.
5. Hottinen T, Mikkola M, Lund P. Evaluation of planar free-breathing polymer electrolyte membrane fuel cell design. *J Power Sources*. 2004;129:68–72. <https://doi.org/10.1016/j.jpowsour.2003.11.012>.
6. Broeck HVD. Fuel cells for transportation. *Energy Storage*, 1980. 230–238. <https://doi.org/10.1016/B978-0-08-025471-5.50024-5>.
7. Kurnia JC, Sasmito AP, Shamim T. Advances in proton exchange membrane fuel cell with dead-end anode operation: a review. *Appl Energy*. 2019;252:113416. <https://doi.org/10.1016/j.apenergy.2019.113416>.
8. Han IS, Jeong J, Shin HK. PEM fuel-cell stack design for improved fuel utilization. *Int J Hydrog Energy*. 2013;38:11996–2006. <https://doi.org/10.1016/j.ijhydene.2013.06.136>.
9. Hwang JJ. Effect of hydrogen delivery schemes on fuel cell efficiency. *J Power Sources*. 2013;239:54–63. <https://doi.org/10.1016/j.jpowsour.2013.03.090>.
10. Yang T, Shi PF. A preliminary study of a six-cell stack with dead-end anode and open-slits cathode. *Int J Hydrog Energy*. 2008;33:2795–801. <https://doi.org/10.1016/j.ijhydene.2008.03.025>.
11. Atkinson RW, Rodgers JA, Hazard MW, Stroman RO, Gould BD. Influence of cathode gas diffusion media porosity on open-cathode fuel cells. *J Electrochem Soc*. 2018;165:1002–11. <https://doi.org/10.1149/2.0041813jes>.
12. Kreesaeng S, Chalermssinsuwan B, Piumsombon P. Effect of channel designs on open-cathode PEM fuel cell performance: a computational study. *Energy Procedia*. 2015;79:733–45. <https://doi.org/10.1016/j.egypro.2015.11.559>.
13. Kiattamrong S, Sripakagorn A. Effects of the geometry of the air flowfield on the performance of an open-cathode PEMFC-transient load operation. *Energy Procedia*. 2015;79:612–9. <https://doi.org/10.1016/j.egypro.2015.11.541>.
14. Zhao C, Li BZ, Xing S, Wei RC, Song HR, Wang HJ. Performance and design optimization of different numbers and bolt torque for air-cooled open-cathode proton exchange membrane fuel cells. *J Power Sources*. 2022;530:231322. <https://doi.org/10.1016/j.jpowsour.2022.231322>.
15. Zhao C, Xing S, Liu W, Wang HJ. Air and H₂ feed systems optimization for open-cathode proton exchange membrane fuel cells. *Int J Hydrog Energy*. 2021;46:11940–51. <https://doi.org/10.1016/j.ijhydene.2021.01.044>.

16. Strahl S, Husar A, Franco AA. Electrode structure effects on the performance of open-cathode proton exchange membrane fuel cells: a multiscale modeling approach. *Int J Hydrog Energy*. 2014;39:9752–67. <https://doi.org/10.1016/j.ijhydene.2014.03.218>.
17. Zhao C, Xing S, Liu W, Wang HJ. Comprehensive anode parameter study for an open-cathode PEMFC. *Energy Fuel*. 2020;34:7582–90. <https://doi.org/10.1021/acs.energyfuels.0c01083>.
18. Xu YM, Chang GF, Zhang JN, Li YY, Xu SC. Investigation of inlet gas relative humidity on performance characteristics of PEMFC operating at elevated temperature. *World Electr Veh J*. 2021;12:110–2. <https://doi.org/10.3390/wevj12030110>.
19. Sachin C, Chinmay C, Kapil S, Alok S, Kapur GS, Ramakumar SSV. Experimental and modelling studies of low temperature PEMFC performance. *Int J Hydrog Energy*. 2020;45:8866–74. <https://doi.org/10.1016/j.ijhydene.2020.01.019>.
20. Yang ZR, Du Q, Jia ZW, Yang CG, Jiao K. Effects of operating conditions on water and heat management by a transient multi-dimensional PEMFC system model. *Energy*. 2019;183:462–76. <https://doi.org/10.1016/j.energy.2019.06.148>.
21. Lu JB, Wei GH, Zhu FJ, Yan XH, Zhang JL. Pressure effect on the PEMFC Performance. *Fuel Cells*. 2019;19:11–220. <https://doi.org/10.1002/fuce.201800135>.
22. Zhang Q, Lin R, Techer L, Cui X. Experimental study of variable operating parameters effects on overall PEMFC performance and spatial performance distribution. *Energy*. 2016;115:550–60. <https://doi.org/10.1016/j.energy.2016.08.086>.
23. Williamson Z, Kim D, Chun DK. Experimental evaluation of cell temperature effects on miniature, air-breathing PEM fuel cells. *Appl Therm Eng*. 2011;31:3761–7. <https://doi.org/10.1016/j.applthermaleng.2011.06.010>.
24. Pahon E, Jemei S, Chabriat JP. Impact of the temperature on calendar aging of an open cathode fuel cell stack. *J Power Sources*. 2021;488:229436. <https://doi.org/10.1016/j.jpowsour.2020.229436>.
25. Hottinen T, Himanen O, Lund P. Performance of planar free-breathing PEMFC at temperatures below freezing. *J Power Sources*. 2006;154:86–94. <https://doi.org/10.1016/j.jpowsour.2005.03.195>.
26. Zeyoudi H, Sasmito AP, Shamim T. Performance evaluation of an open-cathode PEM fuel cell stack under ambient conditions: case study of United Arab Emirates. *Energy Convers Manag*. 2015;105:798–809. <https://doi.org/10.1016/j.enconman.2015.07.082>.
27. Wilson MS, Valerio JA, Gottesfeld S. Low platinum loading electrodes for polymer electrolyte fuel cells fabricated using thermoplastic ionomers. *Electrochim Acta*. 1995;40:355–63. [https://doi.org/10.1016/0013-4686\(94\)00272-3](https://doi.org/10.1016/0013-4686(94)00272-3).
28. Cho E, Ko JJ, Ha HY, Hong SA, Lee KY, Lim TW, Oh IH. Effects of water removal on the performance degradation of PEMFCs repetitively brought to <math><0^{\circ}\text{C}</math>. *J Electrochem Soc*. 2004;151(5):A661. <https://doi.org/10.1149/1.1683580>.
29. Oszcipok M, Zedda M, Riemann D, Geckeler D. Low temperature operation and influence parameters on the cold start ability of portable PEMFCs. *J Power Sources*. 2005;154:404–11. <https://doi.org/10.1016/j.jpowsour.2005.10.035>.
30. Zhang J, Wang C, Zhang A. Experimental study on temperature and performance of an open-cathode PEMFC stack under thermal radiation environment. *Appl Energy*. 2022;311:118646. <https://doi.org/10.1016/j.apenergy.2022.118646>.
31. Atkinson RW, Hazard MW, Rodgers JA, Stroman RO, Gould BD. An open-cathode fuel cell for atmospheric flight. *J Electrochem Soc*. 2017;164:F46–54. <https://doi.org/10.1149/2.0261702jes>.
32. Boukoberine M, Zhou B, Benbouzid M. A critical review on unmanned aerial vehicles power supply and energy management: solutions, strategies, and prospects. *Appl Energy*. 2019;255:113823. <https://doi.org/10.1016/j.apenergy.2019.113823>.
33. Mohamed G, Sayem Z. Analysis of a hydrogen fuel cell-PV power system for small UAV. *Int J Hydrog Energy*. 2016;41:6422–32. <https://doi.org/10.1016/j.ijhydene.2016.02.129>.
34. Emre O, Yalin G. Evaluation of design methodology, limitations, and iterations of a hydrogen fuelled hybrid fuel cell mini UAV. *Energy*. 2020;213:118757. <https://doi.org/10.1016/j.energy.2020.118757>.
35. Pei H, Liu Z, Zhang H, Yu Y, Tu Z, Wan Z. In situ measurement of temperature distribution in proton exchange membrane fuel cell I a hydrogen-air stack. *J Power Sources*. 2013;227:72–9. <https://doi.org/10.1016/j.jpowsour.2012.11.027>.
36. Corbo P, Migliardini F, Veneri O. Experimental analysis of a 20 kW PEM fuel cell system in dynamic conditions representative of automotive applications. *Energy Convers Manag*. 2008;49:2688–97. <https://doi.org/10.1016/j.enconman.2008.04.001>.
37. Xu X, Yang W, Zhuang X, Xu B. Experimental and numerical investigation on effects of cathode flow field configurations in an air-breathing high-temperature PEMFC. *Int J Hydrog Energy*. 2019;44:25010–20. <https://doi.org/10.1016/j.ijhydene.2019.07.237>.
38. Zeng T, Zhang CZ, Huang ZY, Li MX, Chan SH, Li Q, Wu XS. Experimental investigation on the mechanism of variable fan speed control in open cathode PEM fuel cell. *Int J Hydrog Energy*. 2019;44:24017–27. <https://doi.org/10.1016/j.ijhydene.2019.07.119>.
39. China Meteorological Administration. China's wind energy resource assessment report. Beijing: China Meteorological Press. 2006.
40. Jiang Y, Luo Y, Zhao ZG, Zhu JH. Review of research on wind resources changes in China and in the world. *Sci Technol Herald*. 2009;27:96–104. <https://doi.org/10.3321/j.issn:1000-7857.2009.13.019>.
41. Blackadar A. The Beaufort wind scale. *Weatherwise*. 1986;39:278–80. <https://doi.org/10.1080/00431672.1986.9929303>.
42. Meyer Q, Ronaszegi K, Pei-June G, Curnick O. Optimization of air cooled, open-cathode fuel cells: current of lowest resistance and electro-thermal performance mapping. *J Power Sources*. 2015;291:261–9. <https://doi.org/10.1016/j.jpowsour.2015.04.101>.
43. Luo LZ, Huang B, Cheng ZY, Jian QF. Rapid degradation characteristics of an air-cooled PEMFC stack. *Int J Energy Res*. 2020;44:4784–99. <https://doi.org/10.1002/er.5266>.
44. Yan QG, Toghiani H, Causey H. Steady state and dynamic performance of proton exchange membrane fuel cells (PEMFCs) under various operating conditions and load changes. *J Power Sources*. 2006;161:492–502. <https://doi.org/10.1016/j.jpowsour.2006.03.077>.
45. Awad M. Comments on Flow dynamic characteristics in flow field of proton exchange membrane fuel cells. *Int J Hydrog Energy*. 2008;33:1040–51. <https://doi.org/10.1016/j.ijhydene.2012.09.153>.
46. Obeisun OA, Meyer Q, Engebretsen E, Finegan DP, Robinson JB, Hinds G. Study of water accumulation dynamics in the channels of an open-cathode fuel cell through electro-thermal characterization and droplet visualization. *Int J Hydrog Energy*. 2015;40(46):16786–96. <https://doi.org/10.1016/j.ijhydene.2015.07.066>.
47. Huang Z, Jian Q, Zhao J. Thermal management of open-cathode proton exchange membrane fuel cell stack with thin vapor chambers. *J Power Sources*. 2021;485:229314. <https://doi.org/10.1016/j.jpowsour.2020.229314>.
48. Dou ML, Hou M, Liang D, Shen Q, Zhang HB, Lu WT, Shao ZG, Yi BL. Behaviors of proton exchange membrane fuel cells under

oxidant starvation. *J Power Sources*. 2011;196:2759–62. <https://doi.org/10.1016/j.jpowsour.2010.11.005>.

Publisher's Note Springer Nature remains neutral with regard to jurisdictional claims in published maps and institutional affiliations.

Springer Nature or its licensor (e.g. a society or other partner) holds exclusive rights to this article under a publishing agreement with the author(s) or other rightsholder(s); author self-archiving of the accepted manuscript version of this article is solely governed by the terms of such publishing agreement and applicable law.